SHAPE OPTIMIZATION UNDER UNCERTAINTY – A STOCHASTIC PROGRAMMING PERSPECTIVE

SERGIO CONTI*, HARALD HELD*, MARTIN PACH*, MARTIN RUMPF†, AND RÜDIGER SCHULTZ*

Abstract. We present an algorithm for shape-optimization under stochastic loading, and representative numerical results. Our strategy builds upon a combination of techniques from two-stage stochastic programming and level-set-based shape optimization. In particular, usage of linear elasticity and quadratic objective functions permits to obtain a computational cost which scales linearly in the number of *linearly independent* applied forces, which often is much smaller than the number of different realizations of the stochastic forces. Numerical computations are performed using a level-set method with composite finite elements both in two and in three spatial dimensions.

Key Words: Two-stage stochastic programming, shape optimization in elasticity, level-set method.

AMS subject classifications: 49N30, 74P05.

1. Introduction. Uncertainty is a prevailing issue in many, if not most, practical shape optimization problems. In the optimization of elastic structures, one usually deals with volume and in particular surface loadings which are not fixed but vary stochastically over time. Decisions on the shape have to be made before the stochastic forcing is applied. Thus, an optimal structure for the expectation of the stochastic loading does not properly reflect the actual stochastic optimization set up. Indeed, one observes a striking similarity with two-stage stochastic programming. Our work received inspiration from this field and this paper is intended to work out this analogy in the case of shape optimization for linear elastic material laws and stochastic volume and surface loadings.

Optimization under uncertainty depends on information available on the uncertain problem components. At the one end, there are worst-case approaches, as in online or robust optimization [3, 16]. These approaches assume that only the ranges of the uncertain parameters are known, without distributional information. At the other end, stochastic optimization deals with models where uncertainty can be captured by a probability distribution. Stochastic optimization has been analyzed in continuous time, as for example in stochastic dynamic programming or stochastic control [20, 28]. In particular, there exists a rich theory and methodology to treat stochastic uncertainty in (mostly finite-dimensional) mathematical programming models, mainly linear [51], less often linear mixed-integer or nonlinear programming models [14, 48, 57]. In two-stage stochastic programming [18, 35, 49], first-stage decisions must be taken without knowing the realizations of the random data, and then, after observation of the random data, a second-stage (or recourse) decision is taken. The requirement that the first-stage decision must not depend on the future observation is referred to as nonanticipativity. This notion extends accordingly if the two-stage scheme of alternating decision and observation is expanded into a (finite) multistage scheme. For a recent comprehensive overview we refer to [60]. Related work on nonlinear models can be found in optimal design of structural systems under uncertainty, see [42] and references therein. The essential difference to the present work is that design decisions in these contributions vary in Euclidean spaces, while our design decisions are shapes (open sets) in suitable working domains.

Shape optimization under deterministic loading is a well-developed field, which can be seen as an instance of PDE-constrained infinite-dimensional optimization, see e.g. the books [4, 17, 56]; a brief review of the points relevant for us is presented below. We are not aware of two- or multistage stochastic programming approaches in shape optimization, or more generally in PDE constrained optimization. There are, however, recent approaches in shape optimization which generalize the single load assumption. In so–called multiload approaches a fixed (usually small) number of different loading configuration is considered and optimization refers to this set of configurations, see, e.g., [8, 30, 61] and references therein, as well as [13] for an one-dimensional model. In these approaches each evaluation of the objective functional requires a separate computation for each of the possible stochastic forces, which renders them infeasible if the set of possible forces is large, as for example is the case when one aims at approximating a continuous distribution of forces. A more efficient method was derived for a truss model in [12], where it is shown that optimization of the expected compliance is equivalent to a convex problem,

*Department of Mathematics, University of Duisburg-Essen, Lotharstr. 65, D-47048 Duisburg, Germany

†Institute for Numerical Simulation, Rheinische Friedrich-Wilhelms-Universität Bonn, Nussallee 15, 53115 Bonn, Germany

and hence efficiently solvable. This however is based on additional geometrical assumptions, namely, on considering a fixed *ground structure*, and leaving only the thickness of the bars to be optimized. A robust probabilistic approach for the optimization of beam models is discussed in [1], whereas in [43] structural reliability is discussed for beam geometries with uncertain load magnitude. Worst-case situations in a multiload context have also been considered, see, e.g., [15].

The paper is organized as follows. In the next Paragraph 1.1 we formulate the stochastic shape optimization problem considered in this paper. Then in Paragraph 1.2 we review deterministic shape optimization based on a level formulation. Then in paragraph 1.3 we recall finite dimensional, two-stage stochastic optimization to underline the close similarity of the approach to shape optimization to be discussed here. In Section 2 the two-stage shape optimization with stochastic volume and surface loads is introduced, the primal and dual stochastic state equations are investigated in 2.1 and a representation of the stochastic shape gradient is given in 2.2. A finite element discretization for elastic domains described via level sets is discussed in Section 3. In 3.1 we introduce composite finite elements and suitable multigrid methods to apply them for the efficient solution of the discrete primal and dual problem in 3.2, whereas in 3.3 the actual numerical algorithm based on a regularized gradient descent is presented. Finally, in Section 4 we discuss various applications in two and three space dimensions and show corresponding numerical results.

1.1. Setup of the shape optimization problem. In shape optimization one seeks the shape $\mathcal{O}$ of a body which optimizes certain response properties. We shall focus here on optimality criteria which depend on the linear elastic response to applied forces. Therefore we start by describing the elastic problem. Given an admissible shape $\mathcal{O} \subset \mathbb{R}^d$ ($d = 2, 3$) representing the elastic body, the displacement $u : \mathcal{O} \to \mathbb{R}^d$ is determined as the solution of the following system of linear partial differential equations:

$$\begin{aligned} -\operatorname{div}(Ae(u)) &= f(\omega) \quad \text{in } \mathcal{O}\,, \\ u &= 0 \quad \text{on } \Gamma_D\,, \\ (Ae(u))n &= g(\omega) \quad \text{on } \Gamma_N\,, \\ (Ae(u))n &= 0 \quad \text{on } \partial\mathcal{O} \setminus \Gamma_N \setminus \Gamma_D\,. \end{aligned} \tag{1.1}$$

Here, $e(u) = \frac{1}{2}(\nabla u + \nabla u^\top)$ is the linearized strain tensor and $A = (A_{ijkl})_{ijkl}$ the elasticity tensor. We shall for simplicity focus on isotropic materials, where $A_{ijkl} = 2\mu\delta_{ik}\delta_{jl} + \lambda\delta_{ij}\delta_{kl}$, where δ_{ij} denotes the Kronecker symbol and μ, λ the positive Lamé constants of the material. We only consider admissible shapes $\mathcal{O}$ which are subsets of a fixed, bounded working domain $D \subset \mathbb{R}^d$. On $\Gamma_D \subset \partial\mathcal{O}$ we assume homogeneous Dirichlet boundary conditions $u = 0$, and on $\Gamma_N \subset \partial\mathcal{O}$ we assume inhomogeneous Neumann boundary conditions, with $\Gamma_D \cap \Gamma_N = \emptyset$. Both parts of the boundary are kept fixed during the optimization. Precisely, we shall fix a certain open set $\mathcal{O}_* \subset D$, restrict the class of admissible shapes to $\mathcal{O}$ such that $\mathcal{O}_* \subset \mathcal{O} \subset D$, and assume that $\Gamma_D, \Gamma_N \subset \partial\mathcal{O}_* \cap \partial D$. Then necessarily $\Gamma_D, \Gamma_N \subset \partial\mathcal{O}$. Finally, $f(\omega) \in L^2(D; \mathbb{R}^d)$ and $g(\omega) \in L^2(\Gamma_N; \mathbb{R}^d)$ are random volume forces and surface loads, respectively, and ω is a realization on a probability space Ω. Standard results show that for any connected open set $\mathcal{O}$ with Lipschitz boundary and any fixed realization ω the elasticity problem (1.1) has a unique weak solution $u = u(\mathcal{O}, \omega) \in H^1(\mathcal{O}; \mathbb{R}^d)$ [21, 41].
The unique solution to (1.1) can be equivalently characterized as the unique minimizer of a corresponding quadratic variational problem. In fact, $u(\mathcal{O}, \omega)$ minimizes

$$E(\mathcal{O}, u, \omega) := \frac{1}{2}A(\mathcal{O}, u, u) - l(\mathcal{O}, u, \omega) \quad \text{with} \tag{1.2}$$

$$A(\mathcal{O}, \psi, \vartheta) := \int_{\mathcal{O}} A_{ijkl} e_{ij}(\psi) e_{kl}(\vartheta)\, \mathrm{d}x\,, \tag{1.3}$$

$$l(\mathcal{O}, \vartheta, \omega) := \int_{\mathcal{O}} f_i(\omega)\vartheta_i\, \mathrm{d}x + \int_{\partial\mathcal{O}} g_i(\omega)\vartheta_i\, \mathrm{d}\mathcal{H}^{d-1} \tag{1.4}$$

among all u in $H^1_{\Gamma_D}(\mathcal{O}; \mathbb{R}^d) := \{u \in H^1(\mathcal{O}; \mathbb{R}^d) \mid u = 0 \text{ on } \Gamma_D \text{ in the sense of traces}\}$, see [21, 27, 41] for details. Here and below we implicitly sum over repeated Cartesian indices.
As an objective functional $\mathbf{J}$ we consider

$$\mathbf{J}(\mathcal{O}, \omega) = J(\mathcal{O}, u(\mathcal{O}, \omega)) := \int_{\mathcal{O}} j(u(\mathcal{O}, \omega))\, dx + \gamma \int_{\partial\mathcal{O}} \mathrm{d}\mathcal{H}^{d-1}, \tag{1.5}$$

where γ is a nonnegative control parameter. The second term measuring surface area serves as a regularization. We assume that $j(\cdot)$ is linear or quadratic and does not depend explicitly on the realization ω.

A shape optimization problem under uncertainty is then formulated as

$$\text{minimize} \quad \{\mathbb{E}_\omega\left(\mathbf{J}(\mathcal{O},\omega)\right) \,:\, \mathcal{O}\in\mathcal{U}_{ad}\} \tag{1.6}$$

where $\mathcal{U}_{ad}$ is the set of admissible shapes, e.g., $\mathcal{U}_{ad} := \{\mathcal{O}\subset D \,:\, \mathcal{O} \text{ open}, \mathcal{O}_*\subset\mathcal{O}, \text{Per}(\mathcal{O})<\infty\}$. Here and below $\mathbb{E}_\omega(\dots)$ represents the expected value with respect to the probability distribution of the random variables $f(\omega)$, $g(\omega)$.

We emphasize that we solve the elasticity problem only in the physical domain $\mathcal{O}$. This differs from common practice in shape optimization, which is based on solving the elasticity problem on D with very small (but still positive) values of the elasticity constants λ and μ on $D\setminus\mathcal{O}$. For existence results in this context we refer to [10] and references therein. Our approach is closer to physical reality, but brings some technical difficulties. The surface area term in the definition of the cost functional (1.5) ensures rectifiability of the domain boundary for configurations with finite energy but is not expected to guarantee existence of an optimal design. From a theoretical viewpoint, we are unaware of any result for the existence of solutions for the presently-considered shape-optimization problem. From a numerical viewpoint, this requires robust techniques to solve elasticity problems on badly-shaped domains, which are discussed below. Furthermore, numerically different regularization strategies can be considered.

In the optimization problem (1.6) there is a natural information constraint stating that first, and independently of the realizations of $f(\omega), g(\omega)$, the shape $\mathcal{O}$ has to be selected. Then, after observation of $f(\omega), g(\omega)$, (1.1) determines the displacement field $u = u(\mathcal{O},\omega)$, leading to the objective value $\mathbf{J}(\mathcal{O},\omega)$. This manifests the interpretation of (1.6) as a two-stage random optimization problem: In the outer optimization, or first stage, the nonanticipative decision on $\mathcal{O}$ has to be taken. After observation of $f(\omega), g(\omega)$ the second-stage optimization problem is the mentioned variational problem, given $\mathcal{O}$ and ω. This second stage optimization process is neither associated with further stochastic parameters, nor with the optimization of additional material properties. In fact, it consists of the determination of the elastic displacement, which in turn is required for the computation of the elastic energy and the cost functional. Even though there is no additional decision-making involved, the variational structure of the elasticity problem we are solving gives an obvious analogy to the second-stage problem in stochastic programming.

1.2. Deterministic level set based shape optimization. For the readers' convenience and to introduce notation we here briefly sketch the general procedure in deterministic shape optimization, where the volume and surface forces do not depend on a stochastic realization ω. Furthermore, we give an outline of our level set approach.

To get started, we consider variations $\mathcal{O}_v = (\mathrm{Id}+v)(\mathcal{O})$ of a smooth elastic domain $\mathcal{O}$ for a smooth vector field v defined on the working domain D. The shape derivative [23] of the objective functional $\mathbf{J}$ in the direction v takes the form

$$\begin{aligned}\mathbf{J}'(\mathcal{O})(v) &= J_{,\mathcal{O}}(\mathcal{O},u(\mathcal{O}))(v) + J_{,u}(\mathcal{O},u(\mathcal{O}))(u'(\mathcal{O})(v)) \\ &= \int_{\partial\mathcal{O}} (v\cdot n)\left(j(u(\mathcal{O}))+\gamma\, h\right)\,\mathrm{d}\mathcal{H}^{d-1} + \int_{\mathcal{O}} j_{,u}(u(\mathcal{O}))\left(u'(\mathcal{O})(v)\right)\,\mathrm{d}x\,.\end{aligned} \tag{1.7}$$

Here, h denotes the mean curvature on $\partial\mathcal{O}$, defined as the sum of the principal curvatures, and $u'(\mathcal{O})(v)$ denotes the shape derivative of the elastic displacement defined by $u'(\mathcal{O})(v) = \lim_{t\to 0}[u((\mathrm{Id}+tv)\mathcal{O}) - u(\mathcal{O})]/t$.

In order to avoid the need of a separate evaluation of $u'(\mathcal{O})(v)$ for any infinitesimal domain displacement v, we seek a simpler expression for the $J_{,u}$ term. This is obtained by determining the variation of u with v implicitly, through its definition. Precisely, $u(\mathcal{O})$ was defined as the weak solution of (1.1), i. e.,

$$A(\mathcal{O},u(\mathcal{O}),\vartheta) = l(\mathcal{O},\vartheta) \tag{1.8}$$

for all $\vartheta\in H^1_{\Gamma_D}(\mathcal{O};\mathbb{R}^d)$. Differentiating this with respect to the variation v of the domain $\mathcal{O}$ (which in

this entire discussion is assumed to be sufficiently smooth), we get

$$A(\mathcal{O}, u'(\mathcal{O})(v), \vartheta) = l_{,\mathcal{O}}(\mathcal{O}, \vartheta)(v) - A_{,\mathcal{O}}(\mathcal{O}, u(\mathcal{O}), \vartheta)(v) \quad \text{with} \tag{1.9}$$

$$A_{,\mathcal{O}}(\mathcal{O}, \psi, \vartheta)(v) = \int_{\partial\mathcal{O}} (v \cdot n) A_{ijkl} e_{ij}(\psi) e_{kl}(\vartheta) \, \mathrm{d}\mathcal{H}^{d-1} \,, \tag{1.10}$$

$$l_{,\mathcal{O}}(\mathcal{O}, \vartheta)(v) = \int_{\partial\mathcal{O}} (v \cdot n) \, (f_i + g_i \, h + \partial_n g_i) \, \vartheta_i \, \mathrm{d}\mathcal{H}^{d-1} \,, \tag{1.11}$$

We observe that $J_{,u}(\mathcal{O}, u(\mathcal{O}))(\cdot)$ is a linear bounded functional on $L^2(D; \mathbb{R}^d)$. Therefore we can consider the dual problem, and define $p(\mathcal{O}) \in H^1_{\Gamma_D}(D; \mathbb{R}^d)$ to be the solution of

$$A(\mathcal{O}, \vartheta, p(\mathcal{O})) = -J_{,u}(\mathcal{O}, u(\mathcal{O}))(\vartheta) \tag{1.12}$$

for all ϑ in $H^1_{\Gamma_D}(\mathcal{O}; \mathbb{R}^d)$. For the purpose of later reference let us also give a variational interpretation of this dual approach. Equation (1.12) corresponds to the fact that $p(\mathcal{O}) \in H^1_{\Gamma_D}(\mathcal{O}; \mathbb{R}^d)$ minimizes the quadratic functional

$$F(q) = \frac{1}{2} A(\mathcal{O}, q, q) + J_{,u}(\mathcal{O}, u(\mathcal{O}))(q) \tag{1.13}$$

among all $q \in H^1_{\Gamma_D}(\mathcal{O}; \mathbb{R}^d)$. In the strong formulation, we thus ask for a solution p of the system of partial differential equations $-\mathrm{div}\,(Ae(p(\mathcal{O}))) = -j_{,u}(u(\mathcal{O}))$, with $p(\mathcal{O}) = 0$ on Γ_D and $Ae(p(\mathcal{O})) \cdot n = 0$ on $\partial\mathcal{O} \setminus \Gamma_D$. Choosing $\vartheta = u'(\mathcal{O})(v)$ in (1.12) and recalling (1.19), one finally rewrites the shape derivative (1.7) of the objective functional as follows:

$$\begin{aligned}
\mathbf{J}'(\mathcal{O})(v) &= J_{,\mathcal{O}}(\mathcal{O}, u(\mathcal{O}))(v) - A(\mathcal{O}, u'(\mathcal{O})(v), p(\mathcal{O})) \\
&= J_{,\mathcal{O}}(\mathcal{O}, u(\mathcal{O}))(v) - l_{,\mathcal{O}}(\mathcal{O}, p(\mathcal{O}))(v) + A_{,\mathcal{O}}(\mathcal{O}, u(\mathcal{O}), p(\mathcal{O}))(v) \\
&= \int_{\partial\mathcal{O}} (v \cdot n) \big[j(u(\mathcal{O})) + \gamma \, h - (f_i + g_i \, h + \partial_n g_i) \, p_i(\mathcal{O}) \\
&\qquad + A_{ijkl} e_{ij}(u(\mathcal{O})) e_{kl}(p(\mathcal{O})) \big] \, \mathrm{d}\mathcal{H}^{d-1} \,.
\end{aligned} \tag{1.14}$$

In order to permit the topology of the domain $\mathcal{O}$ to change, we consider an implicit description of shapes in terms of a level set function $\phi : D \to \mathbb{R}$. In particular, the elastic body is represented by $\mathcal{O} = \{\phi < 0\} := \{x \in D \,|\, \phi(x) < 0\}$, and its boundary $\partial\mathcal{O}$ corresponds to the zero level set of ϕ, i.e., $D \cap \partial\mathcal{O} = \{\phi = 0\}$. Shape optimization and shape analysis for elastic solids via level set methods has been investigated by various authors [10, 24, 38, 54]. In particular Allaire and co–workers [4, 6, 7, 10] have extensively studied a level set modeling of shapes in two- and three-dimensional structural optimization and compared and combined this approach with homogenization methods. In [9] they recently investigated topological optimization in the context of minimizing the expected elastic stress.

Interface propagation based on level sets was first introduced by Osher and Sethian [45] and since then attracted very much attention due to their enormous flexibility. For a general overview we refer to [44, 53]. If a domain boundary $\partial\mathcal{O}$ propagates with speed v, the evolution of the corresponding level set function ϕ is given by the level set equation $\partial_t \phi + |\nabla\phi| \, v \cdot n = 0$, where $n = \frac{\nabla\phi}{|\nabla\phi|}$ is the field of outer normals on the level sets. In fact, the level set equation identifies variations $s = \partial\phi$ of the level set function with variations $v \cdot n$ of the level sets in direction of the normal n. Even though hypersurfaces are described in the level-set context by functions on the whole domain, suitable implementations lead to efficient numerical algorithms as well [2, 36, 59]. Fairly general shapes can be effectively described and modeled with level sets [40]. Shape sensitive analysis as introduced by Sokolowski and Zolesio [56] can be phrased elegantly in terms of level sets. Let us rewrite the objective functional $\mathbf{J}(\mathcal{O})$ in terms of a level set function ϕ and define

$$\mathcal{J}(\phi) := \mathbf{J}(\{\phi < 0\}). \tag{1.15}$$

Due to the above identification we obtain for the shape derivative of $\mathcal{J}(\phi)$ with respect to a variation s of ϕ (again, working for the moment on smooth domains and away from degeneracies and topological changes)

$$\mathcal{J}'(\phi)(s) = \mathbf{J}'(\{\phi < 0\})(-s \, |\nabla\phi|^{-1} n) \,. \tag{1.16}$$

For the relaxation of the shape functional we now consider a gradient descent

$$\partial_t \phi(t) = -\text{grad}_{\mathcal{G}} \mathcal{J}(\phi)$$

with respect to a metric $\mathcal{G}$ on the space of variations of the level set function ϕ (cf. [47]). This metric ensures smoothness of the descent path and is expected to approximate a regular minimizer from the set of all minimizers. For an overview on optimal design based on level sets and suitable energy descent methods we refer to a recent survey by Burger and Osher [19]. From (1.14) we learn that the support of $\mathbf{J}'(\mathcal{O})(\cdot)$ is contained in $\partial\mathcal{O} \setminus \Gamma_D$. Thus, we take into account a regularized gradient descent, based on the metric

$$\mathcal{G}(\zeta, \xi) = \int_D \zeta\xi + \frac{\rho^2}{2} \nabla\zeta \cdot \nabla\xi \, \mathrm{d}x \,, \tag{1.17}$$

which is related to a Gaussian filter with width ρ. For the time discretization, we consider Armijo rule as a step size control and starting with an initial level set function ϕ^0 we iteratively compute a sequence of level set functions $(\phi^k)_{k=1,\dots}$ given by

$$\mathcal{G}(\phi^{k+1} - \phi^k, \xi) = -\tau \mathcal{J}'(\phi^k)(\xi) \tag{1.18}$$

for all test functions ξ and a sequence of time steps $(\tau^k)_{k=1,\dots}$. In each time step a linear elliptic problem of the type $(\text{Id} - \frac{\rho^2}{2}\Delta)\phi = r$ has to be solved. Alternatively, one might consider a relaxation of shapes described via an evolution of signed distance functions [22, 29]. For the spatial discretization we consider piecewise affine continuous finite element functions on the working domain D. Shape relaxations tend to create fine scale structures and complicated domains $\mathcal{O}$. To evaluate the objective functional itself and the shape derivative the elastic displacement u on $\mathcal{O}$ has to be computed solving the Euler Lagrange equations (1.1) of the inner, elastic minimization subproblem. Here, we apply multilevel composite finite elements introduced by Hackbusch and Sauter [32, 52]. They incorporate the characteristic behavior of the solution on fine scales into the coarse scale shape functions without, necessarily, adding degrees of freedom.

1.3. Two stage stochastic programming revisited. Before we apply two stage stochastic programming to our shape optimization problem, let us recall the basic concepts from finite-dimensional stochastic optimization. Consider the random linear program

$$\min\{c^\top x + q^\top y \ : \ Tx + Wy \ = \ z(\omega), \ \ x \in X, \ y \in Y\} \tag{1.19}$$

for finite dimensional polyhedra X and Y in Euclidean space together with the information constraint

$$\text{decide } x \ \mapsto \ \text{observe } \omega \ \mapsto \ \text{decide } y = y(x, \omega).$$

We assume that the minimum exists; possibly making the spaces larger we can also without loss of generality replace the condition $y \in Y$ by $y \geq 0$ (that is, $y_i \geq 0$ for all i). We also remark that given x and $z(\omega)$ there are multiple solutions y from which we have to select one.
Let us emphasize the two stage characteristic of this optimization problem. Indeed, rewriting (1.19) yields

$$\begin{aligned} &\min_x \left\{ c^\top x + \min_y \{ q^\top y \ : \ Wy \ = \ z(\omega) - Tx, \ y \in Y \} \ : \ x \in X \right\} \\ &= \min\{ c^\top x + \Phi(z(\omega) - Tx) \ : \ x \in X \} \,, \end{aligned} \tag{1.20}$$

where $\Phi(v) := \min\{q^\top y \ : \ Wy = v, \ y \in Y\}$ is the value function of a linear program with parameters on the right-hand side. The cost functional we aim to minimize is $\mathrm{j}(x, \omega) := c^\top x + \Phi(z(\omega) - Tx)$. The representation (1.20) gives rise to understanding the search for a "best" nonanticipative decision x in the initial random optimization problem as the search for a "minimal" member in the family of random variables $\{\mathrm{j}(x, \omega) \ : \ x \in X\}$ where x is seen as an "index" varying in the set X. In a risk-neutral setting, these random variables are ranked by their expectations, leading to the (nonlinear) optimization problem

$$\min\{Q_{I\!E}(x) \ := \ I\!E_\omega \, (\mathrm{j}(x, \omega) \ : \ x \in X\}. \tag{1.21}$$

The straightforward but crucial idea is to detect structural properties and algorithmic possibilities in (1.21) by resorting to the dual of the linear program with value function $\Phi(\cdot)$. Indeed, one observes

$$\Phi(v) \;=\; \min\{q^\top y \,:\, Wy = v,\, y \geq 0\} \;=\; \max\{v^\top y \,:\, W^\top y \leq q\} = \max_{l=1,\cdots,L} d_l^\top v\,, \quad (1.22)$$

where $\{d_l\}_{l=1,\cdots,L}$ denotes the set of vertices of the dual polyhedron $\{y \,:\, W^\top y \leq q\}$, which is assumed compact, and $v = z(\omega) - Tx$. Recalling the cost functional $\mathrm{j}(x,\omega)$, we can rewrite (1.21) and obtain

$$\min\Big\{c^\top x + \sum_{\sigma=1}^{S} \pi_\sigma \max_{l=1,\ldots,L} d_l^\top (z_\sigma - Tx) \;\;:\;\; x \in X\Big\} \quad (1.23)$$

in case of a discrete probability distribution with realizations z_σ and probabilities π_σ for $\sigma = 1,\ldots,S$. Here S is the total number of scenarios. Thus minimizing $Q_{I\!E}$ amounts to minimizing a piecewise linear convex function over a polyhedron. Let us emphasize that in our concrete setup, the functional to be minimized in (1.23) depends linearly on the random variable z, which can be exploited further in the actual numerical minimization.

Algorithmically, two aspects are important: By its very definition, computing $Q_{I\!E}(x)$ in (1.21) would amount to solving $\min\{q^\top y \,:\, Wy = z_\sigma - Tx,\, y \geq 0\}$ for all scenarios z_σ with $\sigma = 1,\ldots,S$, and this again at any new iteration point x. In (1.23) this is prevented by using dual information. Here, the situation is particularly comfortable since cutting planes generated in adaptations of bundle methods, see e.g. [50, 55], capture (at least approximately) information on the objective also locally around iteration points. The second aspect is that (sub)gradient information on $Q_{I\!E}$ is made available by the help of the dual, cf. (1.23).

The facts reviewed above form our guideline for treating shape optimization under uncertainty: Departing from the outlined two-stage model with shape decisions in the first stage and displacements in the second we will formulate an (infinite dimensional) counterpart to the expectation problem (1.21). The variational formulation of the elasticity system will provide an inner optimization problem in the spirit of (1.20). As in (1.22) a duality argument will provide information for the shape derivative. In what follows, the domain $\mathcal{O}$ replaces the variable x, the elastic deformation $u(\mathcal{O},\omega)$ the optimal solution y being a minimizer of the above $\Phi(v)$, where v depends on x and $z(\omega)$. Finally, as a counterpart to the cost functional $\mathrm{j}(x,\omega)$ we consider the objective functional $\mathbf{J}(\mathcal{O},\omega)$. Moreover, as above, in each iteration of a descent method linearity of the elasticity PDE will avoid the solution of as many related PDEs as there are scenarios.

2. Two-Stage Stochastic Programming Formulation of Shape Optimization. We now present our stochastic shape-optimization scheme, which incorporates the techniques from deterministic shape-optimization discussed in Section 1.2 and the two-stage stochastic programming reviewed in Section 1.3. In our setting, the second stage optimization problem is the variational problem of linearized elasticity, where for a fixed elastic domain $\mathcal{O}$ and random state ω one seeks a displacement u which minimizes the energy $E(\mathcal{O},u,\omega)$ defined in (1.2). In turn, the objective functional can be computed from the domain $\mathcal{O}$ and the displacement u, and hence can be seen as a function of $\mathcal{O}$ and the random state ω. We observe the following information constraints:

$$\text{decide } \mathcal{O} \;\mapsto\; \text{observe } \omega \;\mapsto\; \text{compute } u = u(\mathcal{O},\omega)\,.$$

In other words, one first selects a domain $\mathcal{O}$ (like in Section 1.3 one decided for some x), then random volume and boundary forces $f(\omega)$ and $g(\omega)$ are applied (the counterpart of the right hand side $z(\omega)$ in (1.19)), and only at this point the elastic displacement u (the counterpart of the degree of freedom y in (1.19)) and hence the objective functional can be computed. Thus, in analogy to (1.20) we can reformulate the random shape optimization problem in a two-stage optimization manner as follows:

$$\min\Big\{\mathbf{J}(\mathcal{O},\omega) \;:\; u(\mathcal{O},\omega) = \operatorname{argmin}_{u\in H^1_{\Gamma_D}(\mathcal{O};\mathbb{R}^d)} E(\mathcal{O},u,\omega)\Big\}\,.$$

As mentioned above, $\mathcal{O}$ has the role of the first-stage and $u(\mathcal{O},\omega)$ of the second-stage decisions. Finally, the stochastic program

$$\min\Big\{Q_{I\!E}(\mathcal{O}) := I\!E_\omega\left(\mathbf{J}(\mathcal{O},\omega)\right) \;:\; \mathcal{O} \in \mathcal{U}_{ad}\Big\}, \quad (2.1)$$

arises as the "natural" counterpart to (1.21). Replacing the variational problem in (2.1) by its Euler equation enables us to introduce the (dual or) adjoint system needed to effectively compute gradients of the stochastic objective functional.

2.1. Stochastic primal and dual problem. We start from the analysis of the second-stage problem. As illustrated in Section 1.3, in order to determine the shape derivative of the objective function it is convenient to solve both the primal and the dual elastic problem as a counterpart of (1.22) in two stage stochastic programming. Precisely, given $\mathcal{O}$ and ω we seek a primal solution $u(\mathcal{O},\omega) \in H^1_{\Gamma_D}(D;\mathbb{R}^d)$ and a dual solution $p(\mathcal{O},\omega) \in H^1_{\Gamma_D}(D;\mathbb{R}^d)$, such that

$$A(\mathcal{O},u(\mathcal{O},\omega),\vartheta) = l(\mathcal{O},\vartheta,\omega)\,, \tag{2.2}$$
$$A(\mathcal{O},\vartheta,p(\mathcal{O},\omega)) = -J_{,u}(\mathcal{O},u(\mathcal{O},\omega))(\vartheta) \tag{2.3}$$

for all $\vartheta \in H^1_{\Gamma_D}(D;\mathbb{R}^d)$. The function $u(\mathcal{O},\omega)$ entering the dual problem is the solution to the primal problem. Let us emphasize that as in (1.22) both the primal and the dual state solve variational problems, in fact (1.2) and (1.13), respectively.

A key simplification in the solution of these equations arises from the general fact that the solution of a linear problem depends linearly on the data. We phrase this fact first in general terms, and then discuss the implications in our setting. Let $A_{\mathcal{O}} : H^1_{\Gamma_D} \to H^{-1}_{\Gamma_D}(D;\mathbb{R}^d)$ be the elliptic operator induced by the quadratic form $A(\mathcal{O},\cdot,\cdot)$, in fact $A_{\mathcal{O}}(u)(\vartheta) = A(\mathcal{O},u,\vartheta)$. By the positivity of the elastic coefficients, for any Lipschitz, connected domain $\mathcal{O}$, and under the assumption that $\Gamma_D \subset \partial\mathcal{O}$ has positive $(d-1)$-dimensional measure, the operator $A_{\mathcal{O}}$ is bounded and coercive on the Hilbert space $H^1_{\Gamma_D}(D;\mathbb{R}^d)$, and therefore invertible. This implies that for any $l \in H^{-1}_{\Gamma_D}(D;\mathbb{R}^d)$ one can find a unique solution u to $A_{\mathcal{O}}(u,\vartheta) = l(\vartheta)$, namely, $u = A_{\mathcal{O}}^{-1}l$. Therefore both (2.2) and (2.3) have a unique solution, which depends linearly on the right-hand side.

We now consider the specific case of interest here, namely, the dependence of u and p on ω. The crucial point is that the left-hand side of both equations, i.e., the quadratic form $A(\mathcal{O},\cdot,\cdot)$, does not depend on ω. The right-hand side depends on ω only through f, g and u, and this dependence is linear. Here it is important that the integrand j entering the objective function is linear or quadratic. We shall now exploit this fact in order to obtain an efficient algorithm, which does not require to solve (2.2) and (2.3) for every ω, but only for a representative subset (a "basis").

We start from the primal problem (2.2). Since the right-hand side is linear in the forces f and g, and A does not depend on ω, the solution u depends linearly on the forces f and g. In order to make this more explicit, assume that f and g are random combinations of finitely many forces $f^1,\dots,f^K \in L^2(D;\mathbb{R}^d)$ and $g^1,\dots,g^M \in H^1(D;\mathbb{R}^d)$, respectively, i.e.,

$$f(\omega) = \sum_{k=1}^{K} \alpha_k(\omega) f^k, \qquad g(\omega) = \sum_{m=1}^{M} \beta_m(\omega) g^m.$$

Here the $\alpha_k(\omega)$ and $\beta_m(\omega)$ are stochastic coefficients. For later convenience we assume that $\sum_{k=1}^{K} \alpha_k(\omega) = \sum_{m=1}^{M} \beta_k(\omega) = 1$. (This can always be achieved by a rescaling of the coefficients of f^k's and g^m's, such that their corresponding sums are both smaller than 1. Adding two virtual loads equal to zero, we easily can ensure the equality sign.) We assume that ω follows a discrete distribution with scenarios ω_σ and probabilities π_σ with $\sigma = 1,\dots,S$ ($\sum_{\sigma=1}^{S} \pi_\sigma = 1$); continuous distributions can be recovered in the limit $S \to \infty$. For any pair $(k,m) \in \{1,\dots,K\} \times \{1,\dots,M\}$ let $u^{km}(\mathcal{O})$ be the solution to the elasticity system $(1.1)_{km}$, which is (1.1) with right-hand sides f^k, g^m. Then, for any $\sigma = 1,\dots,S$,

$$\bar{u}(\mathcal{O},\omega_\sigma) \;:=\; \sum_{k=1}^{K}\sum_{m=1}^{M} \alpha_k(\omega_\sigma)\beta_m(\omega_\sigma) u^{km}(\mathcal{O}) \tag{2.4}$$

solves (1.1) for $\omega = \omega_\sigma$. In the numerical implementation, we confine to $K+M$ displacements, where each of them corresponds either to a single volume force or a single boundary force and vanishing components with respect to all other forces. To simplify the presentation, we consider here an over–determined system of $K\,M$ spanning displacements. This is a substantial algorithmic shortcut, in the

case that the discretization parameter of the probability measure S is larger than the sum of the $K + M$ effective base forces.
An analogous argument applies to the dual problem (2.3). We first determine, for each pair $(k, m) \in \{1, \dots, K\} \times \{1, \dots, M\}$, the solution $p^{km}(\mathcal{O})$ of the basis problem

$$A(\mathcal{O}, \vartheta, p^{km}(\mathcal{O})) = -J_{,u}(\mathcal{O}, u^{km}(\mathcal{O}))(\vartheta)\,, \text{ for all } \vartheta \in H^1_{\Gamma_D}(D; \mathbb{R}^d)\,. \tag{2.5}$$

Since j depends linearly or quadratically on u, the dependence of $j_{,u}$ on u is linear (possibly trivial). Therefore (2.4) and the above introduced normalization implies

$$J_{,u}(\mathcal{O}, \bar{u}(\mathcal{O}, \omega_\sigma))(\vartheta) = \sum_{k=1}^{K} \sum_{m=1}^{M} \alpha_k(\omega_\sigma)\beta_m(\omega_\sigma) J_{,u}(\mathcal{O}, u^{km}(\mathcal{O}))(\vartheta)$$

and linearity of the inverse operator $A^{-1}_{\mathcal{O}}$ gives

$$\bar{p}(\mathcal{O}, \omega_\sigma) = \sum_{k=1}^{K} \sum_{m=1}^{M} \alpha_k(\omega_\sigma)\beta_m(\omega_\sigma) p^{km}(\mathcal{O})\,. \tag{2.6}$$

Obviously, $\bar{p}(\mathcal{O}, \omega_\sigma)$ is the weak solution $\bar{p}$ of $-\mathrm{div}\,(Ae(\bar{p})) = -j'(\bar{u}(\mathcal{O}, \omega_\sigma))$ on the domain $\mathcal{O}$ with $\bar{p} = 0$ on Γ_D and $Ae(\bar{p}) \cdot n = 0$ on $\partial\mathcal{O} \setminus \Gamma_D$.

2.2. Shape gradient in the stochastic optimization problem. Now, with the primal solution $\bar{u}(\mathcal{O}, \omega_\sigma)$ for a particular realization ω_σ at hand, the stochastic program (2.1) can be rewritten as follows

$$\begin{aligned} \min \Big\{ \gamma \int_{\partial\mathcal{O}} \mathrm{d}\mathcal{H}^{d-1} + \sum_{\sigma=1}^{S} \pi_\sigma \int_{\mathcal{O}} j(\bar{u}(\mathcal{O}, \omega_\sigma))\, dx \;:\; \\ \bar{u}(\mathcal{O}, \omega_\sigma) := \sum_{k=1}^{K} \sum_{m=1}^{M} \alpha_k(\omega_\sigma)\beta_m(\omega_\sigma) u^{km}(\mathcal{O}),\ \sigma = 1, \dots, S \Big\}. \end{aligned} \tag{2.7}$$

Using the primal solution for the elastic deformation $\bar{u}(\mathcal{O}, \omega_\sigma)$ and the dual solution $\bar{p}(\mathcal{O}, \omega_\sigma)$ for any realization ω_σ we deduce the stochastic shape derivative (1.7) of the objective functional $\mathbf{J}(\mathcal{O}, \omega_\sigma)$ and achieve, from (1.14),

$$\begin{aligned} \mathbf{J}'(\mathcal{O}, \omega_\sigma)(v) &= J_{,\mathcal{O}}(\mathcal{O}, \bar{u}(\mathcal{O}, \omega_\sigma))(v) - l_{,\mathcal{O}}(\mathcal{O}, \bar{p}(\mathcal{O}, \omega_\sigma))(v) \\ &\quad + A_{,\mathcal{O}}(\mathcal{O}, \bar{u}(\mathcal{O}, \omega_\sigma), \bar{p}(\mathcal{O}, \omega_\sigma))(v) \\ &= \int_{\partial\mathcal{O}} (v \cdot n) \big(j(\bar{u}(\mathcal{O}, \omega_\sigma)) + \gamma\, h - (f_i(\omega_\sigma) + g_i(\omega_\sigma)\, h + \partial_n g_i)\, \bar{p}_i(\mathcal{O}, \omega_\sigma) \\ &\qquad + A_{ijkl} e_{ij}(\bar{u}(\mathcal{O}, \omega_\sigma)) e_{kl}(\bar{p}(\mathcal{O}, \omega_\sigma)) \big)\, \mathrm{d}\mathcal{H}^{d-1}\,. \end{aligned} \tag{2.8}$$

Finally, the shape derivative of our actual stochastic cost functional, namely of the expectation of the cost $Q_{I\!E}(\mathcal{O})$ in case of S scenarios $(\omega_\sigma)_{\sigma=1,\cdots,S}$, is given by

$$Q'_{I\!E}(\mathcal{O})(v) = I\!E_\omega \left(\mathbf{J}'(\mathcal{O}, \omega)(v) \right) = \sum_{\sigma=1}^{S} \pi_\sigma J'(\mathcal{O}; \omega_\sigma)(v)\,. \tag{2.9}$$

In the algorithm this shape derivative can be used as a descent direction. Thereby, first the $K\,M$ primal and dual base states are computed. These allow the efficient evaluation of the effective deformations $\bar{u}(\mathcal{O}, \omega_\sigma)$ and the effective dual states $\bar{p}(\mathcal{O}, \omega_\sigma)$ for a set of S scenarios ω_σ with S usually much larger than $K\,M$.

3. Multiscale finite element implementation. In this section we detail the concrete numerical algorithm and consider a finite element approach for the representation of the level set function ϕ on the working domain D, which implicitly describes the discrete elastic domain $\mathcal{O}$ as the sublevel set of the discrete level set function. The elastic state equations for u^{km} and the corresponding set of dual problems for p^{km} are discretized as well with finite elements. Here, we pick up the composite finite element approach originally proposed by [32] and investigated in the level set context for complicated 3D geometries in [37]. Finally, we will discuss the time step control used in our descent scheme.

3.1. Finite element spaces. Without any restriction we suppose our working domain D to be a hexahedron ($d = 3$) or a rectangle ($d = 2$), respectively. In a first step, a hierarchical grid is generated based on successive subdivision of hexahedrons (rectangles) into 8 (4) equally sized child hexahedrons (rectangles). Next, each cell of the resulting fine grid is split into 6 tetrahedra (2 triangles) such that a regular simplicial grid $\mathcal{T}_h$ of the domain D is obtained. We denote the simplicial elements of this grid by $T \in \mathcal{T}_h$, and the set of nodes of by $\mathcal{N}_h = \{X_i\}_{i\in I_h}$ with a corresponding index set I_h. Let us emphasize that we do not represent this simplicial grid explicitly. Instead access to element data is implicitly encoded in look up tables. Here, h indicates the grid size. Let $\mathcal{V}_h$ be the space of continuous, piecewise affine functions on $\mathcal{T}_h$ with the canonical basis $\{\Phi_i\}_{i\in I_h}$, given by $\Theta_i(X_j) = \delta_{ij}$. In the sequel, discrete variables will always be capitalized whereas continuous ones will be lowercase. Now, we consider a discrete level set function $\Phi(x) = \sum_{i\in I_h} \Phi_i\Theta_i(x)$. As a consequence, the discrete domain $\mathcal{O}_h = \{x \in D \,|\, \Phi(x) < 0\}$ is polygonal. This algorithmic advantage justifies the use of a tetrahedral grid. A solution of the state equation (2.2) and the dual problem (2.3) is defined on the elastic domain only. Here, we explicitly work with a void phase $D \setminus \mathcal{O}$ and, at variance with [5, 11], we do not consider a softer elastic material outside of actual elastic body $\mathcal{O}$ to be optimized. Thus, we have to define suitable finite element spaces on the discrete elastic domain $\mathcal{O}_h$ implicitly described by a level set function $\Phi \in \mathcal{V}_h$. A straightforward mesh generation based on a marching cube type algorithm [39, 58] leads to badly shaped tetrahedra with a significant impact on the condition number of the linear systems to be solved. Explicit grid generation would require a regular remeshing of the boundary $\partial\mathcal{O}_h$ followed by the actual meshing algorithm in $\mathcal{O}_h \subset \mathbb{R}^d$ [25, 46]. Both steps are fairly complicated in case of general elastic domains and result in non hierarchical, unstructured meshes which do not allow for a multilevel algorithm for the discrete PDE problems. To avoid these drawbacks we construct a suitable composite finite element space. In contrast to explicit meshing approaches, the geometry is encoded in the design of the basis functions which still correspond to grid nodes of the regular underlying grid. In fact, given a basis function $\Theta_i \in \mathcal{V}_h$ whose support intersects the discrete elastic domain $\mathcal{O}_h$, we define the corresponding composite finite element basis function $\Theta_i^{\text{cfe}}(x) = \chi_{\mathcal{O}_h}(x)\Theta_i(x)$ selecting the part of the old basis function contained in the elastic domain [32]. Here $\chi_{\mathcal{O}_h}$ denotes the characteristic function of the discrete domain $\mathcal{O}_h$. Let us remark that there are also degrees of freedom at nodes outside the actual domain as long as the support of the corresponding basis function interests $\mathcal{O}_h$. Collecting all these basis functions we obtain the composite finite element space

$$\mathcal{V}_h^{\text{cfe}} := \{\Theta_i^{\text{cfe}}(x) = \chi_{\mathcal{O}_h}(x)\Theta_i(x) \,|\, \operatorname{supp}\Theta_i \cap \mathcal{O}_h \neq \emptyset\}$$

and the resulting nodal index set I_h^{cfe} is a subset of the index set I_h. Hence, far from the domain boundary the basis functions coincide with the standard basis functions, whereas in the vicinity of the boundary, the standard basis is modified to resolve the domain geometry. Finally, let us incorporate boundary data and define $\mathcal{V}_{h,\Gamma_D}^{\text{cfe}} = (\mathcal{V}_h^{\text{cfe}})^3 \cap H^1_{\Gamma_D}(D;\mathbb{R}^d)$ as the space of discrete vector valued functions which vanish on the Dirichlet boundary Γ_D. For the sake of simplicity, we assume here Γ_D to be resolved on the underlying regular grid. Thus, no special treatment of the Dirichlet boundary condition in the construction of the composite finite elements [33] is required. Indeed, to conserve the Dirichlet boundary condition we furthermore freeze the level set function ϕ in a small neighbourhood of the Dirichlet boundary Γ_D and the Neumann boundary Γ_N on which the surface load is applied. Hence, in this region the body still behaves elastic but does not undergo any optimization. As basis functions for the vector valued problem we consider $\Theta_i^{\text{cfe}} e_j$ with $i \in I_h^{\text{cfe}}$ and $1 \le j \le d$.

3.2. Discrete primal and dual solutions. Given the composite finite element space $\mathcal{V}_{h,\Gamma_D}^{\text{cfe}}$ we can solve the primal and the dual problem numerically. Explicitly, the discrete primal solutions are defined as the finite element functions $U^{km} \in \mathcal{V}_{h,\Gamma_D}^{\text{cfe}}$ solving

$$A(\mathcal{O}_h, U^{km}, \Theta) = l^{km}(\mathcal{O}_h, \Theta) \tag{3.1}$$

for all $\Theta \in \mathcal{V}_{h,\Gamma_D}^{\text{cfe}}$, where $l^{km}(\mathcal{O}_h,\Theta) := \int_{\mathcal{O}_h} f_i^k\Theta_i \,\mathrm{d}x + \int_{\partial\mathcal{O}_h} g_i^m\Theta_i \,\mathrm{d}\mathcal{H}^{d-1}$ for $1 \le k \le K$ and $1 \le m \le M$. The corresponding set of dual solutions are those functions $P^{km} \in \mathcal{V}_{h,\Gamma_D}^{\text{cfe}}$, for which

$$A(\mathcal{O}_h, \Theta, P^{km}) = -J_{,u}(\mathcal{O}_h, U^{km})(\Theta) \tag{3.2}$$

for all $\Theta \in \mathcal{V}_{h,\Gamma_D}^{\text{cfe}}$. For the variation of the cost functional J with respect to the discrete elastic displacement U we obtain $J_{,u}(\mathcal{O}_h, U^{km})(\Theta) = \int_{\mathcal{O}_h} j_{,u}(U^{km})(\Theta)\,\mathrm{d}x$. Due to assumption that $j(\cdot)$ is

a linear or quadratic polynomial, the resulting integrant is at most quadratic and can be integrated exactly using a Gauss quadrature rule. In case of the compliance cost functional $J(\mathcal{O}, u(\mathcal{O}, \omega)) = l^{km}(\mathcal{O}, u^{km}, \omega) + \gamma \int_{\partial\mathcal{O}} \mathrm{d}\mathcal{H}^{d-1}$, we derive as usual from (3.1) the representation $J_{,u}(\mathcal{O}_h, U^{km})(\Theta) = A(\mathcal{O}_h, U^{km}, \Theta) = \int_{\mathcal{O}_h} A_{ijkl} e_{ij}(U^{km}) e_{kl}(\Theta)\,\mathrm{d}x$. The numerical solution of (3.1) and (3.2) both require numerical quadrature for the assembly of the stiffness matrix $(A(\mathcal{O}_h, \Theta_i e_j, \Theta_r e_s))_{i,r\in I_h^{\mathrm{cfe}}, 1\le j,s\le d}$ and the right hand side vectors $(l^{km}(\mathcal{O}_h, \Theta_r e_s))_{r\in I_h^{\mathrm{cfe}}, 1\le s\le d}$ and $(-J_{,u}(\mathcal{O}_h, U^{km})(\Theta_r e_s))_{r\in I_h^{\mathrm{cfe}}, 1\le s\le d}$, respectively. For this purpose, on simplices of the original mesh which are intersected by the domain boundary $\partial\mathcal{O}_h$ a local, virtual grid is generated. Based on a look up table the cells generated by the marching cube type method in the construction of the composite finite elements are subdivided into simplices. On these simplices and on the simplices within $\mathcal{O}_h$ not intersected by the domain boundary a one point, center of mass quadrature rule is applied. The evaluation of the boundary integral $\int_{\partial\mathcal{O}_h} g_s^m \Theta_r \,\mathrm{d}\mathcal{H}^{d-1}$ is treated analogously.
As long as the discrete domain $\mathcal{O}_h$ is connected in the following discrete sense: for every node X_i with $i \in I_h^{\mathrm{cfe}}$ there is a chain of nodes $(X_j)_{j=0,\cdots,n}$ with $j \in I_h^{\mathrm{cfe}}$ such that $[X_j, X_{j+1}]$ is an edge of $\mathcal{T}_h$, $X_0 = X_i$ and X_n is a node on Γ_D we easily verify that there exist unique solutions U^{km} and P^{km} of (3.1) and (3.2), respectively. The resulting symmetric linear systems of equations are solved with a conjugate gradient method for $d = 2$ and with a multigrid method for $d = 3$. In general a still high condition number for the corresponding linear system of equations on the finest grid level will reflect the badly shaped support of single composite basis functions. Here, in particular the multigrid method leads to convergence rates which are independent of the grid size h and - for a wide range of problems - the geometric complexity of the domain. For the multigrid solver, we first recursively construct coarse grid matrices and right hand sides. Here, the underlying hierarchical grid induces a canonical projection operator for any grid level to the next finer one generated by the cell subdivision. Let us emphasize that this applies not only for the hierarchical hexahedral grid but analogously for the associated simplicial mesh as well. Based on the projection operator a standard Galerkin projection [31] is applied both for the matrices and the right hand sides. We then use a multigrid method with V cycles and symmetric Block-Gauß-Seidel iterations as a smoother. Thereby, we gather the 3 spatial components of the solution at a grid node and apply the Gauß-Seidel iterations on the resulting 3×3 blocks. In the applications considered here, 3 pre- and post-smoothing steps in the V cycle turned out to be a reasonable choice. For details on the composite finite element approach and the multigrid method we refer to [37].

3.3. Discrete gradient descent algorithm. The numerical relaxation of the shape functional is based on the time discretized, regularized gradient descent scheme given in (1.18) and applied to the spatially discrete stochastic shape functional

$$Q_{I\!E,h}(\mathcal{O}_h) := I\!E_\omega\left(\mathcal{J}(\Phi, \omega)\right) = \sum_{\sigma=1}^{S} \pi_\sigma \mathcal{J}(\Phi, \omega_\sigma) \tag{3.3}$$

where the shape functional $\mathcal{J}$ for a discrete level set function Φ is defined in straightforward way by $\mathcal{J}(\Phi, \omega_\sigma) := \mathbf{J}(\{\Phi < 0\}, \omega_\sigma)$ for any realization ω_σ. Here, for the ease of presentation we notationally do not distinguish continuous and discrete shape functionals, in fact in what follows discrete shape functionals always involve the corresponding discrete solution of the state equation. For an initial level set function $\Phi^0 \in \mathcal{V}_h$ we iteratively compute a sequence of level set functions $(\Phi^k)_{k=1,\cdots}$ given by

$$\mathcal{G}(\Phi^{k+1} - \Phi^k, \Xi) = -\tau I\!E_\omega\left(\mathcal{J}'(\Phi^k, \omega)(\Xi)\right) \tag{3.4}$$

for all $\Xi \in \mathcal{V}_h$. Hence, in every time step the vector $\left(I\!E_\omega\left(\mathcal{J}'(\Phi^k, \omega)(\Psi_i)\right)\right)_{i\in I_h}$ of variations of the expectation of the objective functional $\mathcal{J}$ in all basis directions Ψ_i for $i \in I_h$ has to be evaluated. Furthermore, one has to solve the linear system of equations resulting from a standard finite element discretization of $\mathcal{G}$. As already discussed the time step τ is chosen according to a simple variant of the Armijo step size control. Indeed, given a constant $\beta \in (0, 1)$ we accept a timestep τ if the condition

$$I\!E_\omega\left(\mathcal{J}(\Phi^{k+1}, \omega)\right) - I\!E_\omega\left(\mathcal{J}(\Phi^k, \omega)\right) \le -\beta\mathcal{G}(\Phi^{k+1} - \Phi^k, \Phi^{k+1} - \Phi^k)$$

is satisfied, otherwise the timestep is reduced.
Let us now detail the evaluation of $\mathcal{J}'(\Phi)(\Xi)$ in the spatially discrete setting. For any scenario of the stochastic loading ω_σ with $\sigma = 1, \ldots, S$ we obtain a discrete effective displacement $\bar{U}(\mathcal{O}_h, \omega_\sigma) \in$

$\mathcal{V}^{\text{cfe}}_{h,\Gamma_D}$ and a effective dual solution $\bar{P}(\mathcal{O}_h,\omega_\sigma) \in \mathcal{V}^{\text{cfe}}_{h,\Gamma_D}$ as the following linear combinations of U^{km} and P^{km} (cf. (2.4), (2.6)), respectively:

$$\bar{U}(\mathcal{O}_h,\omega_\sigma) = \sum_{k=1}^{K}\sum_{m=1}^{M} \alpha_k(\omega_\sigma)\beta_m(\omega_\sigma) U^{km}(\mathcal{O}_h)\,,$$
$$\bar{P}(\mathcal{O}_h,\omega_\sigma) = \sum_{k=1}^{K}\sum_{m=1}^{M} \alpha_k(\omega_\sigma)\beta_m(\omega_\sigma) P^{km}(\mathcal{O}_h)\,.$$

Given the discrete primal solution $\bar{U}(\mathcal{O}_h,\omega_\sigma)$ the variation of the objective functional (cf. (1.5))

$$\mathcal{J}(\Phi,\omega_\sigma) = \int_{\mathcal{O}_h} j(\bar{U}(\mathcal{O}_h,\omega_\sigma))\,dx + \gamma \int_{\partial\mathcal{O}_h} \mathrm{d}\mathcal{H}^{d-1}$$

for a particular realization ω_σ of the stochastic loading and a shape domain $\mathcal{O}_h$ implicitly defined by the discrete level set function Φ (that is, $\mathcal{O}_h = \{\Phi < 0\}$) can be computed as follows (cf. (1.16) and (2.8)):

$$\begin{aligned}\mathcal{J}'(\Phi,\omega_\sigma)(\Xi) &= \mathbf{J}'(\mathcal{O}_h,\omega_\sigma)(-\Xi\,|\nabla\Phi|^{-1}N)\\ &= \int_{\partial\mathcal{O}_h} (-\Xi|\nabla\Phi|^{-1})\Big(j(\bar{U}(\mathcal{O}_h,\omega_\sigma)) + \gamma\, H\\ &\qquad - (f_i(\omega_\sigma) + g_i(\omega_\sigma)\, H + \partial_N g_i(\omega_\sigma))\ \bar{P}_i(\mathcal{O}_h,\omega_\sigma)\\ &\qquad + A_{ijkl} e_{ij}(\bar{U}(\mathcal{O}_h,\omega_\sigma)) e_{kl}(\bar{P}(\mathcal{O}_h,\omega_\sigma))\Big)\ \mathrm{d}\mathcal{H}^{d-1}\,. \end{aligned} \tag{3.5}$$

Here, N denotes the outer normal on $\partial\mathcal{O}_h$ and H a discrete mean curvature function on $\partial\mathcal{O}_h$. As a suitable approximation we consider N, H to be piecewise affine on $\partial\mathcal{O}_h$ and on each vertex X on $\partial\mathcal{O}_h$ the discrete mean curvature vector $H\,N$ is defined as the gradient vector of the area functional with respect to the position of the vertex (cf. [26] for the resulting formula and the relation to the continuous mean curvature). For the numerical integration we apply a Gauss quadrature of degree 4. Hence, the integration is exact as long as f and g are (piecewise) affine functions on $\mathbb{R}^d$. Finally, the discrete counterpart of the shape derivative of our actual stochastic cost functional, namely the expectation of the discrete cost functional $Q_{I\!E,h}(\mathcal{O}_h)$ in case of S scenarios $(\omega_\sigma)_{\sigma=1,\cdots,S}$ (cf. (3.3)) is given by

$$Q'_{I\!E,h}(\mathcal{O}_h)(V) = I\!E_\omega\left(\mathcal{J}'(\Phi,\omega)(\Xi)\right) = \sum_{\sigma=1}^{S} \pi_\sigma \mathcal{J}'(\Phi,\omega_\sigma)(\Xi)\,, \tag{3.6}$$

where $V = -\Xi|\nabla\Phi|^{-1}N$ is the normal variation corresponding to the variation Ξ of the level set function Φ. In the algorithm this shape derivative can be used as a descent direction. In any step of the considered time-discrete gradient descent (3.4) one has to compute for the current discrete domain $\mathcal{O}_h$ once the $K\,M$ discrete primal base deformations $U^{km}(\mathcal{O}_h)$ and the corresponding discrete dual base states $P^{km}(\mathcal{O}_h)$. From these, we can efficiently compute the effective deformations $\bar{U}(\mathcal{O},\omega_\sigma)$ and the effective dual states $\bar{P}(\mathcal{O},\omega_\sigma)$ for a possibly very large set of scenarios $\{\omega_\sigma \,|\, \sigma = 1,\cdots,S\}$, and using (3.5) and (3.6) we then evaluate the stochastic descent direction.

4. Computational Results. As discussed above the major characteristic of two stage stochastic shape optimization investigated here is that one first decides the domain $\mathcal{O}$ and then the stochastic loading is observed. Hence, we expect the resulting optimal shapes to differ significantly from those obtained in case of an optimization for the load straightforwardly computed as the expected value of the stochastic loads. In what follows we consider shape optimization applications in two and three dimensions which in particular reflect this consideration. Let us assume a vanishing volume load $f(\omega)$ and Neumann boundary conditions $g(\omega)$ with support Γ_N. As explained above, we assume neither Γ_D nor Γ'_N not to be modified in the actual shape optimization. Indeed, we choose $7h$ as the size of this neighborhood of Γ_D and Γ_N, where the level set function is kept fixed. As objective function, we take into account a sum of the expectation of the compliance load $\int_{\Gamma_N} g(\omega)\cdot u(\mathcal{O},\omega)\,\mathrm{d}\mathcal{H}^{d-1}$ and the weighted volume $\eta\int_{\partial\mathcal{O}}\mathrm{d}\mathcal{H}^{d-1}$ of the structure, where η is a positive constant.

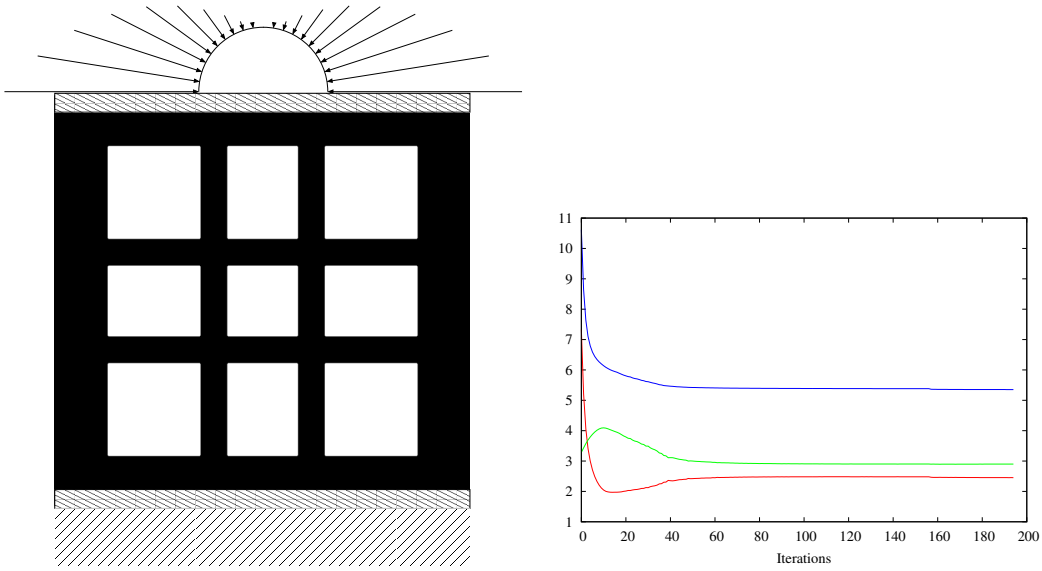

FIG. 4.1. *The initial domain considered in the computation of the optimal shapes in Fig. 4.2 and Fig. 4.3 is depicted on the left. On the right the different contributions to the objective function are plotted over the number of iterations. The upper curve shows the robust decay of the objective functional, whereas the lower curve and the middle curve display the evolution and the interplay of the compliance functional and the enclosed volume term, respectively.*

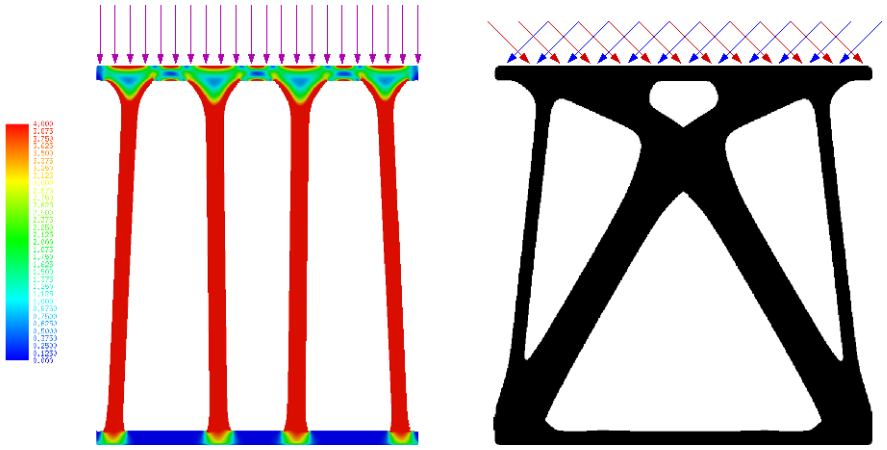

FIG. 4.2. *A direct comparision of two scale stochastic optimization and deterministic optimization for an averaged load is shown. On the right, a stochastically optimal shape is rendered together with the two underlying load scenarios ω_1 and ω_2 on the upper plate, with surface loads $g(\omega_1)$ and $g(\omega_2)$ both with probability $\frac{1}{2}$. On the left the optimal shape colorcoded with the von Mises stress is drawn for a deterministic load $\frac{1}{2}g(\omega_1) + \frac{1}{2}g(\omega_2)$.*

4.1. 2D-Carrier Plate. The first application in 2D is a carrier plate, where we optimize the shape of the carrier construction between a floor slap, whose lower boundary is assumed to be the Dirichlet boundary, and the upper plate, on which the loading is applied. Fig. 4.1 depicts the initial shape and a sketch of a particular instance of the stochastic loading on the upper plate. Figures 4.2, 4.3, and 4.4 show results obtained by the stochastic optimization algorithm presented here. Each realization of the stochastic load is spatially uniform on the upper plate, realizations only differ by the direction of the force. Hence, two base loads g^1 and g^2 are required to span a load space containing all realizations of the stochastic load. Hence $m = 2$, whereas S ranges from 2 in Fig. 4.2 to 20 in Fig. 4.3 and 21 in Fig. 4.4. In Fig. 4.3 a slightly non symmetric set of stochastic scenarios is taken into account, whereas the stochastic load configuration in Fig. 4.4 is symmetric. The resulting optimal domains reflect this break of symmetry. Both figures show on the single stochastically optimal shape the von Mises stress distribution for different load scenarios. For the stochastic optimization result in Fig. 4.2, we have evaluated the relative error in the stress when refining the underlying grid once. Explicitly

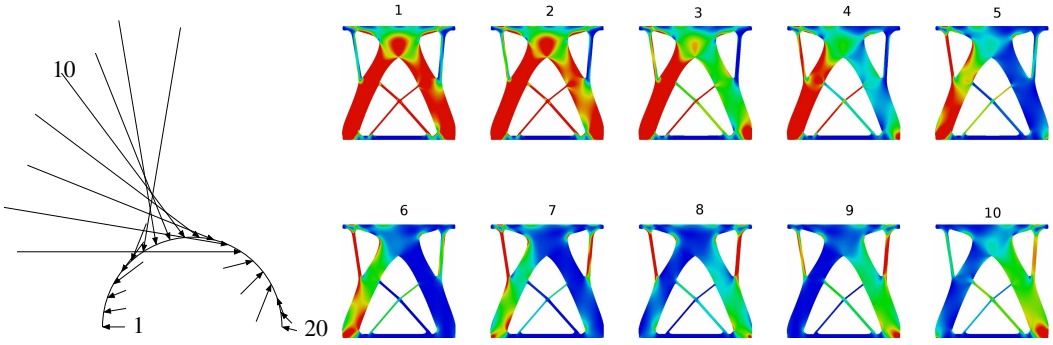

FIG. 4.3. *Stochastic shape optimization based on* 20 *scenarios is depicted. On the left the different loads* $g(\omega_\sigma)$ *with probabilities* π_σ *are sketched. Each arrow represents one scenario where the arrow length is determined by the corresponding force intensity weighted with the probability* π_σ *of the corresponding scenario. On the right the von Mises stress distribution is color coded on the optimal shape for* 10 *out of the* 20 *realization of the stochastic loading. Due to the non symmetric loading configuration the resulting shape is non symmetric as well. In particular the right carrier is significantly thicker than the left one, whereas the connecting diagonal stray pointing up right is thinner than the one point down left.*

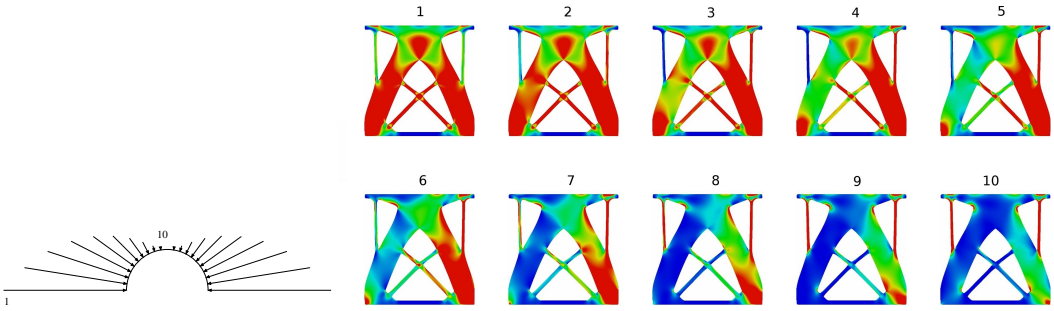

FIG. 4.4. *Results for a symmetric load configuration with* 21 *scenarios, to be contrasted with those reported with an non symmetric configuration in Fig. 4.3. Again on the left the configuration is sketched and on the right the von Mises stress distribution in plotted in case of the first* 10 *scenarios.*

we obtain a relative error $\int_{\mathcal{O}} \left[A_{ijkl}e_{ij}\left(\bar{U}_h(\mathcal{O}) - \bar{U}_{\frac{h}{2}}(\mathcal{O})\right)\right]^2 \mathrm{d}x / \int_{\mathcal{O}} \left[A_{ijkl}e_{ij}(\bar{U}_h(\mathcal{O}))\right]^2 \mathrm{d}x$ of about 0.25 percent. Here $\bar{U}_h(\mathcal{O})$ is the solution for the grid size $h = 2^{-8}$ and $\bar{U}_{\frac{h}{2}}(\mathcal{O})$ the corresponding solution on grid size $h = 2^{-9}$ for the same discrete domain $\mathcal{O}$.

4.2. 2D-Cantilever. The second application deals with shape optimization of a 2D cantilever. The initial domain and the optimal shape in case of deterministic loading are shown in Fig. 4.5. Here the cantilever is fixed on the left side and a downward pointing force is applied on the right. In Fig. 4.6 the dependence of the computed optimal shape on the initial domain is depicted. In Fig. 4.8 we focus on the coefficient in front of the volume penalty term and its impact on the optimal shape. A stochastic counterpart is presented in Fig. 4.9 with 21 different scenarios pulling in different directions. Again the realizations of the stochastic load on the smaller plate on the right are spatially uniform. Thus, the space of realization is two dimensional and we can choose $m = 2$.

The subset of the domain Ω, which does not undergo an optimization but is still treated as elastic material is indicated by the hatched box texture in Fig. 4.1 and Fig.4.5. The diameter of the initial domain is 0.9 and the Lamé coefficients in all instances are $\lambda = 40$ and $\mu = 40$. For the parameters in the objective functional we choose $\eta = 8$ in the application in figures 4.2, 4.3, and 4.4, whereas $\eta = 0.3$ in the case of Fig. 4.5. Here, instead of a regularizing surface area term we consider an iterative regularization strategy based on a weaker morphological operator applied during the gradient descent. In all 2D computations the underlying grid is a uniform grid with 257×257 nodes, the discrete primal and dual state equation are solved using a conjugate gradient approach. Furthermore, we take into account $\beta = 0.2$ for the parameter in the Armijo rule and halfen the step size as required. Finally, we set $\rho = 6h$ for the computations in Figures 4.3 and 4.4 and $\rho = 4h$ in Figures 4.2 and 4.5, where ρ is the filter parameter in the regularized gradient descent. As mentioned above, we regularize the discrete shape boundary after a couple of iterations applying the morphological operator $D(s)E(2s)D(s)$, where $D(\cdot)$ and $E(\cdot)$

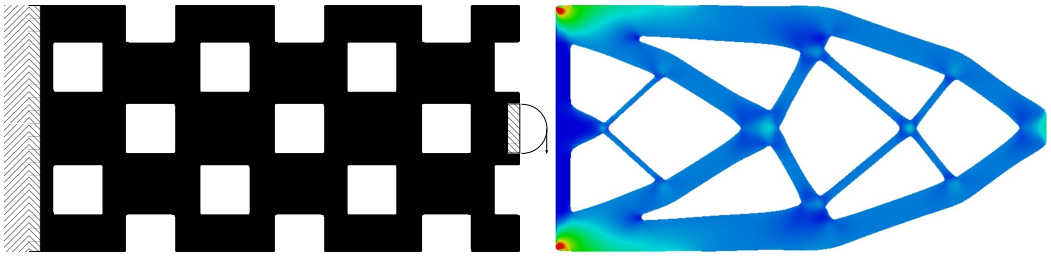

FIG. 4.5. *The initial domain for the computation in case of a cantilever geometry is rendered on the left. The left boundary is a Dirichlet boundary where the cantilever is attached to a vertical wall. The center part of the right boundary is the support Γ_N of the a boundary force, which is a deterministic downward-pointing force in this sketch. The resulting optimal shape computed by the proposed level-set algorithm is plotted on the right and color coded with the von Mises stress. The corresponding stochastic case is reported in Fig. 4.9.*

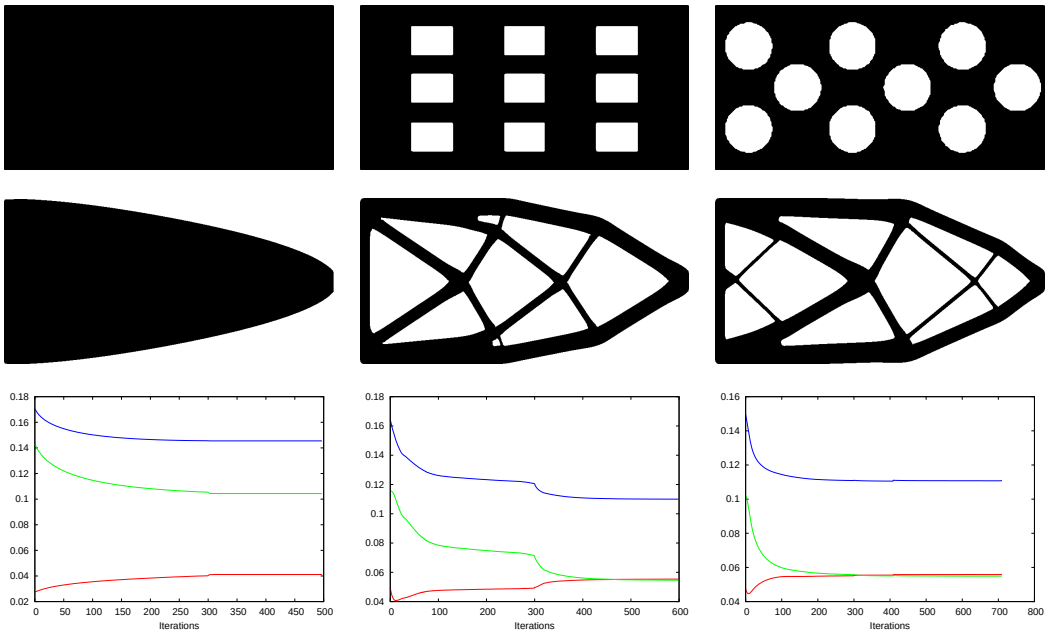

FIG. 4.6. *Results for different initial shapes for the deterministic cantilever computation (see Fig. 4.5). The top row shows the intial guess. The corresponding optimal shapes and energy plots are depicted in the second and third row, respectively. In all cases, η is fixed to 0.3. The middle and right simulation results are obviously local minima with values of the cost functional that are fairly close, as indicated by the error plot.*

are discrete Dilation and Erosion operators, respectively. These operators are implemented via a fast marching method [53]. We set $s = 0.5h$ for the width parameter of these operators. Starting from the initial configuration, the decay of the different energy contributions is plotted already on the right hand side in Fig. 4.1. The underlying stochastic scenario is shown in Fig.4.4.

4.3. VSS and EVPI. As stochastic programs are known to be computationally hard to solve, the question arises whether the additional effort pays off compared to solving simpler deterministic problems. There are two common concepts to measure the quality of the stochastic solution: the *Value of the Stochastic Solution* (VSS) and the *Expected Value of Perfect Information* (EVPI) (see [18] for details). We computed these two values for the instance shown in Fig. 4.2. The optimal objective value of the *recourse problem* (2.1) is denoted by RP, and we consider the following deterministic program, which is called *expected value problem*:

$$\mathrm{EV} := \min \Big\{ \mathbf{J}(\mathcal{O}, \bar{\omega}) \ : \ \mathcal{O} \in \mathcal{U}_{ad} \Big\},$$

where $\bar{\omega}$ indicates that all occuring random variables are substituted by their expectations. Let $\mathcal{O}_{\mathrm{EV}} \in \arg\min\{\mathbf{J}(\mathcal{O}, \bar{\omega}) \ : \ \mathcal{O} \in \mathcal{U}_{ad}\}$. Note that in our example, $\mathcal{O}_{\mathrm{EV}}$ is shown in Fig. 4.2 on the left. Next, we

can define the *expected result of using the EV solution* as EEV $:= \sum_{\sigma=1}^{S} \pi_\sigma \mathbf{J}(\mathcal{O}_{\mathrm{EV}}, \omega_\sigma)$, which finally leads to the VSS given by VSS $=$ EEV $-$ RP. For our particular instance, we have VSS $= 53.68$, or 94 % of the EEV.
To compute the EVPI, we have to compute the so-called *wait-and-see* solution (WS). If $\mathcal{O}_\sigma$ for $\sigma = 1, \ldots, S$ denote the solutions to the many problems

$$\min \Big\{ \mathbf{J}(\mathcal{O}, \omega_\sigma) \ : \ \mathcal{O} \in \mathcal{U}_{ad} \Big\}, \quad \sigma = 1, \ldots, S,$$

(and there are as many of those as scenarios), then WS is defined to be WS $:= \sum_{\sigma=1}^{S} \pi_\sigma \mathbf{J}(\mathcal{O}_\sigma, \omega_\sigma)$, and EVPI $:=$ RP $-$ WS. For our instance, we obtained EVPI $= 0.24$. Finally, we directly compared in Fig. 4.7 the values of the cost functional on the two different optimal shapes computed by our algorithm shown in Fig. 4.3 and Fig. 4.4 for both stochastic load scenarios. Even though the shapes visually do not differ too much, a clear preference is demonstrated for the shape optimized with respect to particular stochastic load configuration.

	$\mathcal{O}_1$	$\mathcal{O}_2$
objective from Fig. 4.3	4.32398	4.4342
objective from Fig. 4.4	5.54182	5.35328

FIG. 4.7. *Let $\mathcal{O}_1$ denote the optimal shape from Fig. 4.3, and $\mathcal{O}_2$ the one from Fig. 4.4. The table shows the cost functionals arising from the different stochastic loadings shown in Fig. 4.3 and Fig. 4.4, respectively, evaluated at $\mathcal{O}_1$ and $\mathcal{O}_2$.*

4.4. 3D-Cantilever. Finally, we consider a 3D cantilever, as a generalization of the problem considered in the first example in 2D. On one side a disk shaped plate is fixed on a wall prescribing zero Dirichlet conditions. On the other side a small rectangular plate opposite to the center of the disk is considered as Neumann boundary loaded with different deterministic and stochastic boundary forces. Fig. 4.10 shows the optimal designs in case of a single deterministic load, and for four and eight stochastic loading scenarios. Furthermore, the energy decay during the numerical relaxation of the shape functional is depicted. As initial shape we have considered a 3D version of the initial 2D shape shown in Fig. 4.1. Fig. 4.11 displays a color coding of the von Mises stress distribution on the optimal shape in the stochastic setting with eight equally probable and equally distributed loads scenarios.
Here, we choose $\eta = 1$ for the volume penalization parameter and the elastic behaviour is described by the Lame coefficients $\lambda = 40$ and $\mu = 40$ for a structure diameter of the order 1. The parameters involved in the Armijo step control are the same as those in the 2D applications. The underlying grid is a regular grid with 128^3 nodes. The shape optimization is first performed on a 64^3 grid. Then the level set function is prolongated to the next finer grid level. Before the gradient descent of the shape functional is released a morphological smoothing operator $D(s)E(2s)D(s)$ is applied. Here, as in the 2D case $D(s)$ and $E(s)$ represent discrete dilation and erosion operators, implemented based in a fast marching algorithm in 3D. As width parameter we select $s = 0.45h$. The filter parameter in the regularized gradient descent is $\rho = 2.5h$. A multigrid method for the numerical solution of the discrete primal and dual problem is applied.

Outlook. Our approach of using two–stage stochastic optimization with the Lamé equation as a variational problem does not only link stochastic shape optimization to two stage stochastic programming. Indeed it offers the flexibility to go beyond expected value optimization and addresses risk aversion. To this end, the expectation in (2.1) is replaced by suitable risk measures such as *expected excess* and *excess probability*. The resulting optimal shapes will significantly depend on the chosen risk measure. Furthermore, we included results on a combination of level set and topological shape optimization which can be extended to the case of uncertain loadings (cf. Fig. 4.12). For a detailed discussion of these issues we refer to a forthcoming publication [34].

Acknowledgements. This work was supported by the Deutsche Forschungsgemeinschaft through the Schwerpunktprogramm 1253 *Optimization with Partial Differential Equations*.

References.

[1] S. ADALI, JR. J.C. BRUCH, I.S. SADEK, AND J.M. SLOSS, *Robust shape control of beams with load uncertainties by optimally placed piezo actuators*, Structural and Multidisciplinary Optimization, 19 (2000), pp. 274–281.

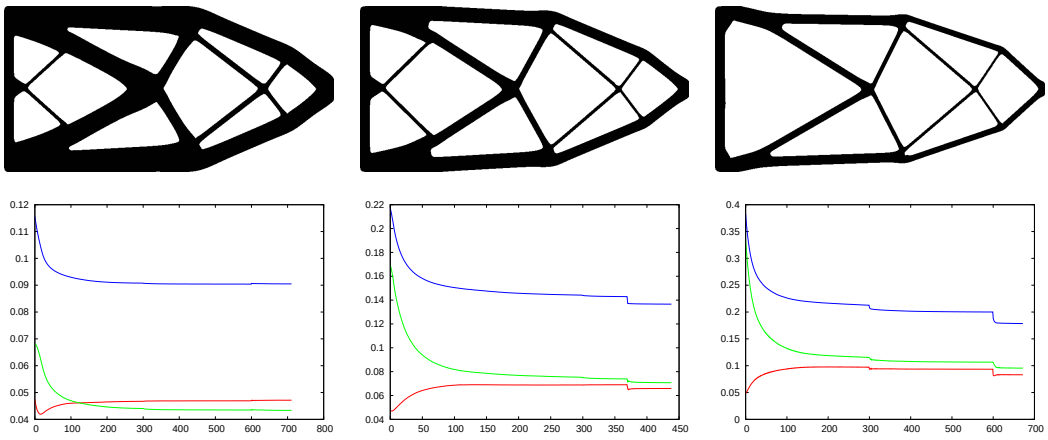

FIG. 4.8. *Results for variations of the volume penalization parameter η. In all shown test runs, the initial shape shown in Fig. 4.6 on the right was used. From left to right, the optimal solutions correspond to the choices $\eta = 0.2, \eta = 0.5, \eta = 1$.*

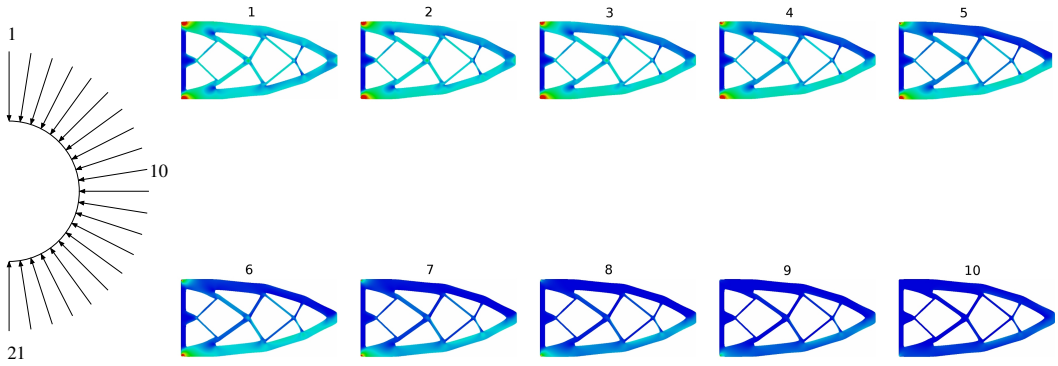

FIG. 4.9. *Stochastic shape optimization in the cantilever case with 21 scenarios. The different loads $g(\omega_\sigma)$ with probabilities π_σ are sketched on the left. The von Mises stress distribution is color coded on the stochastically optimal shape for 10 out of the 21 scenarios.*

[2] D. ADALSTEINSSON AND J. A. SETHIAN, *A fast level set method for propagating interfaces*, Journal of Computational Physics, 118 (1995), pp. 269–277.

[3] S. ALBERS, *Online algorithms: a survey*, Mathematical Programming, 97 (2003), pp. 3–26.

[4] G. ALLAIRE, *Shape optimization by the homogenization method*, vol. 146 of Applied Mathematical Sciences, Springer-Verlag, New York, 2002.

[5] G. ALLAIRE, *Structural optimization using topological and shape sensitive via a level set method*. lecture, 2005.

[6] G. ALLAIRE, E. BONNETIER, G. FRANCFORT, AND F. JOUVE, *Shape optimization by the homogenization method*, Numerische Mathematik, 76 (1997), pp. 27 – 68.

[7] G. ALLAIRE, DE F. GOURNAY, F. JOUVE, AND A.-M. TOADER, *Structural optimization using topological and shape sensitivity via a level set method*, Tech. Report 555, Ecole Polytechnique, Centre de Mathematiques appliquees, UMR CNRS 7641, 91128 Palaiseau Cedex (France), October 2004.

[8] G. ALLAIRE AND F. JOUVE, *A level-set method for vibration and multiple loads structural optimization*, Comput. Methods Appl. Mech. Engrg., 194 (2005), pp. 3269–3290.

[9] G. ALLAIRE, F. JOUVE, AND H. MAILLOT, *Topology optimization for minimum stress design with the homogenization method*, Struct Multidisc Optim, 28 (2004), pp. 87 – 98.

[10] G. ALLAIRE, F. JOUVE, AND A.-M. TOADER, *Structural optimization using sensitivity analysis and a level-set method*, Journal of Computational Physics, 194 (2004), pp. 363–393.

[11] ——, *Structural optimization using sensitivity analysis and a level-set method*, Journal of computational physics, 194 (2004), pp. 363–393.

[12] F. ALVAREZ AND M. CARRASCO, *Minimization of the expected compliance as an alternative*

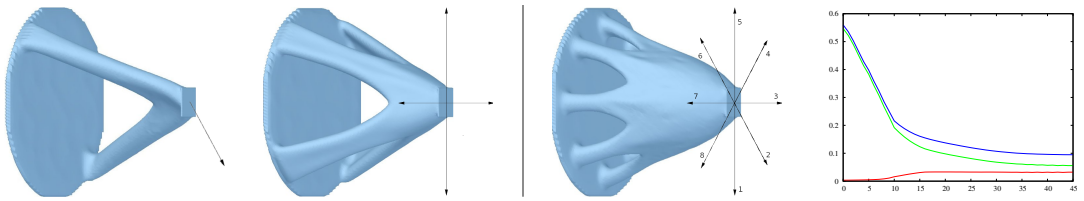

FIG. 4.10. *From left to right the optimal shapes in the deterministic approach and the stochastic optimization approach for* 1, 4, *and* 8 *scenarios are shown. The arrows represent the different involved loads* $g(\omega_\sigma)$ *for varying scenario indices* σ*. On the right the energy decay is shown for the* 8 *scenario configuration. Again the upper curve represents the total value of the objective functional, the middle one the enclosed volume term and the lower one the compliance functional.*

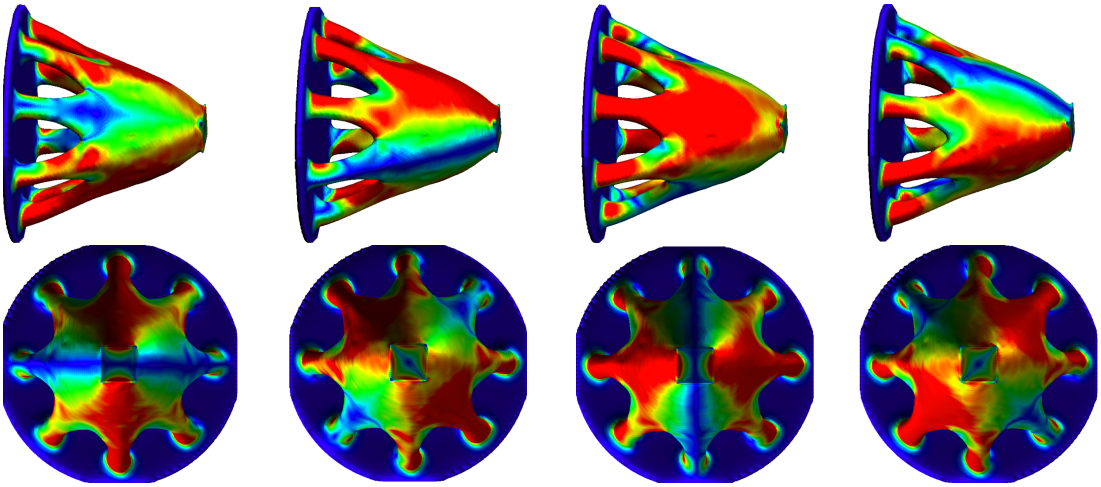

FIG. 4.11. *The optimal design in the case of stochastic shape optimization for the cantilever problem with 8 scenerios is depicted. From left to right 4 scenerios are color coded with the von Mises stress in a consecutive clockwise ordering with respect to the sketch of the loads in Fig. 4.10. The upper and the lower row show the shape geometry under different perspectives.*

approach to multiload truss optimization, Struct. Multidiscip. Optim., 29 (2005), pp. 470–476.

[13] P. ATWAL, *Kontinuumstheorie fr eine diskrete Mikrostruktur zwecks Formoptimierung*, Diplomarbeit, Universitt Duisburg-Essen, (2006).

[14] F. BASTIN, C. CIRILLO, AND PH. TOINT, *Convergence theory for nonconvex stochastic programming with an application to mixed logit*, Math. Program., 108 (2006), pp. 207–234.

[15] A. BEN-TAL, M. KOČVARA, A. NEMIROVSKI, AND J. ZOWE, *Free material design via semidefinite programming: the multiload case with contact conditions*, SIAM J. Optim., 9 (1999), pp. 813–832.

[16] A. BEN-TAL AND A. NEMIROVSKI, *Robust Optimization - methodology and applications*, Mathematical Programming, 92 (2002), pp. 453–480.

[17] M. P. BENDSØE, *Optimization of structural topology, shape, and material*, Springer-Verlag, Berlin, 1995.

[18] J. R. BIRGE AND F. LOVEAUX, *Introduction to Stochastic Programming*, Springer, New York, 1997.

[19] M. BURGER AND S. J. OSHER, *A survey on level set methods for inverse problems and optimal design*, European Journal of Applied Mathematics, 16 (2005), pp. 263–301.

[20] F. R. CHANG, *Stochastic Optimization in Continuous Time*, Cambridge University Press, Cambridge, 2004.

[21] P. G. CIARLET, *Mathematical Elasticity, Volume I: Three-Dimensional Elasticity*, North-Holland, 1988.

[22] M.C. DELFOUR AND J.P. ZOLÉSIO, *Oriented distance funtion and its evolution equation for initial sets with boundary*, SIAM Journal on Control and Optimization, 42, No. 6 (2004), pp. 2286 – 2304.

[23] M. C. DELFOUR AND J.P ZOLÉSIO, *Geometries and Shapes: Analysis, Differential Calculus and*

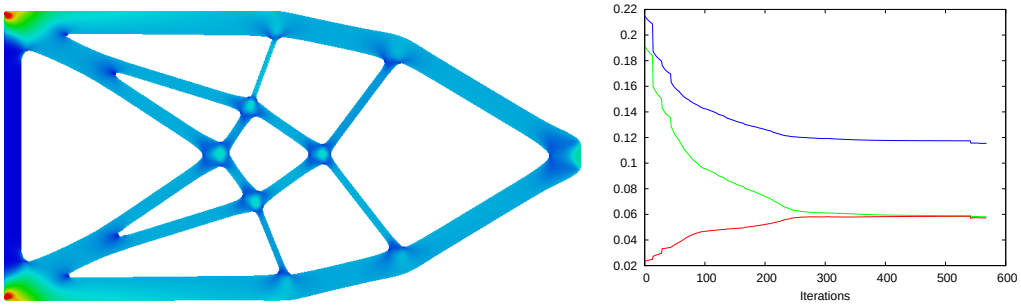

FIG. 4.12. *The optimal shape for a cantilever problem with deterministic loading is computed based on combined level set and topogical derivative approach. A relaxation step with respect to the topological derivative is considered in every* 15*th step of a general shape gradient descent method (left). Furthermore, the corresponding energies, i.e. the total value of the objective function, the enclosed volume, and the compliance functional, are plotted on the right.*

Optimization, Adv. Des. Control 4, SIAM, Philadelphia, 2001.

[24] G. P. DIAS, J. HERSKOVITS, AND F. A. ROCHINHA, *Simultaneous shape optimization and nonlinear analysis of elastic solids*, Computational Mechanics, (1998).

[25] QIANG DU AND DESHENG WANG, *Tetrahedral mesh generation and optimization based on centroidal Voroni tesselations*, International Journal for Numerical Methods in Engineering, 56 (2003), pp. 1355–1373.

[26] G. DZIUK, *An algorithm for evolutionary surfaces*, Numer. Math., 58 (1991), pp. 603–611.

[27] L. C. EVANS, *Partial differential equations*, vol. 19 of Graduate Studies in Mathematics, American Mathematical Society, Providence, RI, 1998.

[28] W. H. FLEMING AND R. W. RISHEL, *Deterministic and Stochastic Optimal Control*, Springer, New York, 1975.

[29] J. GOMES AND O. FAUGERAS, *Reconciling distance functions and level sets*, in Scale-Space Theories in Computer Vision. Second International Conference, Scale-Space '99, Corfu, Greece, September 1999, M. Nielsen, P. Johansen, O. F. Olsen, and J. Weickert, eds., Lecture Notes in Computer Science; 1682, Springer, 1999, pp. 70–81.

[30] J. M. GUEDES, H. C. RODRIGUES, AND M. P. BENDSØE, *A material optimization model to approximate energy bounds for cellular materials under multiload conditions*, Struct. Multidiscip. Optim., 25 (2003), pp. 446–452.

[31] W. HACKBUSCH, *Multi-Grid Methods and Applications*, vol. 4 of Springer Series in Computational Mathematics, Springer, 1985.

[32] W. HACKBUSCH AND S. SAUTER, *Composite finite elements for the approximation of PDEs on domains with complicated micro-structures*, Numerische Mathematik, 75 (1997), pp. 447–472.

[33] W. HACKBUSCH AND S. A. SAUTER, *Composite finite elements for problems with complicated boundary. Part III: Essential boundary conditions*, tech. report, Universität Kiel, 1997.

[34] H. HELD, M. HINTERMÜLLER, M. RUMPF, AND R. SCHULTZ, *Risk averse topology optimization*, in preparation, (2008).

[35] P. KALL AND S.W. WALLACE, *Stochastic Programming*, Wiley, Chichester, 1994.

[36] C.-Y. KAO, S. OSHER, AND Y.-H. TSAI, *Fast sweeping methods for static Hamilton-Jacobi equations*, SIAM Journal on Numerical Analysis, 42 (2005), pp. 2612–2632.

[37] F. LIEHR, T. PREUSSER, M. RUMPF, S. SAUTER, AND L. O. SCHWEN, *Composite finite elements for 3D image based computing*, Submitted to Computing and Visualization in Science, (2007).

[38] Z. LIU, J. G. KORVINK, AND R. HUANG, *Structure topology optimization: Fully coupled level set method via femlab*, Structural and Multidisciplinary Optimization, 29 (2005), pp. 407 – 417.

[39] W. E. LORENSEN AND H. E. CLINE, *Marching cubes: A high resolution 3D surface construction algorithm*, Computer Graphics, 21 (1987), p. 163.

[40] R. MALLADI AND J. A. SETHIAN, *An O(N log N) algorithm for shape modeling*, in Proceedings of National Academy of Sciences, USA, vol. 93 (18), 1996, pp. 9389–9392.

[41] J. E. MARSDEN AND T. J. R. HUGHES, *Mathematical foundations of Elasticity*, Prentice–Hall, Englewood Cliffs, 1983.

[42] K. MARTI, *Stochastic Optimization Methods*, Springer, Berlin, 2005.
[43] R.E. MELCHERS, *Optimality-criteria-based probabilistic structural design*, Structural and Multidisciplinary Optimization, 23 (2001), pp. 34–39.
[44] S. OSHER AND R. FEDKIW, *Level set methods and dynamic implicit surfaces*, vol. 153 of Applied Mathematical Sciences, Springer-Verlag, New York, 2003.
[45] S. J. OSHER AND J. A. SETHIAN, *Fronts propagating with curvature dependent speed: Algorithms based on Hamilton–Jacobi formulations*, Journal of Computational Physics, 79 (1988), pp. 12–49.
[46] S. J. OWEN, *A survey of unstructured mesh generation technology*, in Proceedings of the 7th International Meshing Roundtable, Dearborn, Michigan, 1998, Sandia National Laboratories, pp. 239–267.
[47] MARTIN PACH, *Levelsetverfahren in der Shapeoptimierung*, diploma thesis, University Duisburg, 2005.
[48] T. PENNANEN, *Epi-convergent discretizations of multistage stochastic programs*, Mathematics of Operations Research, 30 (2005), pp. 245–256.
[49] A. PRÉKOPA, *Stochastic Programming*, Kluwer, Dordrecht, 1995.
[50] A. RUSZCZYŃSKI, *Some advances in decomposition methods for stochastic linear programming*, Annals of Operations Research, 85 (1999), pp. 153–172.
[51] A. RUSZCZYŃSKI AND A. SHAPIRO, eds., *Handbooks in Operations Research and Management Sciences, 10: Stochastic Programming*, Elsevier, Amsterdam, 2003.
[52] S. SAUTER, *Vergröberung von Finite-Elemente-Räumen*. Habilitationsschrift, Universität Kiel, 1997. Habilitation.
[53] J. A. SETHIAN, *Level Set Methods and Fast Marching Methods*, Cambridge University Press, 1999.
[54] J. A. SETHIAN AND A. WIEGMANN, *Structural boundary design via level set and immersed interface methods*, Journal of Computational Physics, 163 (2000), pp. 489 – 528.
[55] R. M. VAN SLYKE AND R. J. B. WETS, *L-shaped linear programs with application to optimal control and stochastic programming*, SIAM Journal of Applied Mathematics, 17 (1969), pp. 638–663.
[56] J. SOKOLOWSKI AND J.-P. ZOLÉSIO, *Shape sensitivity analysis*, Springer, 1992, ch. Introduction to shape optimization.
[57] M.C. STEINBACH, *Tree-sparse convex programs*, Mathematical Methods of Operations Research, 56 (2002), pp. 347–376.
[58] G. M. TREECE, R. W. PRAGER, AND A. H. GEE, *Regularized marching tetrahedra: improved iso-surface extraction*, Computers and Graphics, 23 (4) (1999), pp. 583–598.
[59] J. TSITSIKLIS, *Efficient algorothms for globally optimal trajectories*, IEEE Transactions on Automatic Control, 40 (1995), pp. 1528–1538.
[60] S. W. WALLACE AND W. T. ZIEMBA, *Applications of Stochastic Programming*, vol. MPS-SIAM Series on Optimization, SIAM and MPS, Philadelphia, 2005.
[61] C. ZHUANG, Z. XIONG, AND H. DING, *A level set method for topology optimization of heat conduction problem under multiple load cases*, Comput. Methods Appl. Mech. Engrg., 196 (2007), pp. 1074–1084.